

Decay of  $^{133}\text{Pr}$  and structure of  $^{133}\text{Ce}$ 

M. S. Rapaport,\* D. Bucurescu,† C. F. Liang, and P. Paris

*Centre de Spectrométrie Nucléaire et de Spectrométrie de Masse, F-91405 Orsay, France*

(Received 22 June 1990)

Decay of on-line mass-separated  $^{133}\text{Pr}$  sources were carried out.  $\gamma$ , x-ray, conversion-electron singles and time-multiscale, and  $\gamma$ - $\gamma$ - $t$  and  $e^-$ - $\gamma$ - $t$  measurements were used to deduce the  $^{133}\text{Pr}$  decay scheme with 20 levels up to 1881 keV. The low-energy excitation structure of  $^{133}\text{Ce}$  is compared with predications of interacting boson-fermion model calculations.

## I. INTRODUCTION

Systematic studies of the neutron-deficient ( $N < 82$ ) even-even Ce ( $Z = 58$ ) isotopes indicate that the ground-state quadrupole deformation<sup>1</sup> increases as the neutron number decreases. The values of  $\epsilon_2$  were extracted from  $2+$  level energies and lifetime measurements. For the  $4+$  and  $2+$  levels, the ratios for their energies and their transition strengths indicate for the light cerium isotopes ( $N < 74$ ) good axial deformation and possible triaxiality for the  $N > 74$  isotopes. The structure of the Ce isotope, which is of interest in this work, is expected to be related to the coupling of a single-particle state to a  $^{132}\text{Ce}$  or  $^{134}\text{Ce}$  core. Recently, in an in-beam study,<sup>2</sup> triaxiality was concluded for the yrast band built on the  $h_{11/2}$   $[514]_{\frac{9}{2}}^-$  Nilsson orbital from the large energy splitting of its opposite signature components.

Little experimental data on the decay of  $^{133}\text{Pr}$  ( $T_{1/2} = 6.5$  min) to  $^{133}\text{Ce}$  exist at present. Two isomeric states were reported for  $^{133}\text{Ce}$ : low spin ( $I^\pi = \frac{1}{2}^+$  with  $T_{1/2} = 97$  min) and high spin ( $\frac{9}{2}^-$  with  $T_{1/2} = 4.9$  h).<sup>3</sup> The spin values have been measured directly by the atomic-beam magnetic resonance method,<sup>4</sup> but conflicting results were reported for their relative energy.<sup>3,4</sup> In the extensive in-beam reaction study<sup>2</sup> the detailed high-spin level structure of  $^{133}\text{Ce}$  was described and the high-spin isomer was located 39 keV above the low-spin isomer. The reported  $^{133}\text{Pr}$  decay scheme,<sup>3</sup> made of six levels plus five tentative levels and one spin parity assignment, is in great part inconsistent with the present data.

The present paper describes the experimental study of the low-energy low-spin levels of  $^{133}\text{Ce}$  populated in the decay of mass-separated  $^{133}\text{Pr}$ . The excitation structure is then compared with the predictions of the interacting boson-fermion model calculations.

## II. EXPERIMENTAL METHOD

A target of 10-g natural cerium was bombarded with a 280-MeV  $^3\text{He}$  beam from the Orsay IPN synchrocyclotron. The beam intensity was in the range 1–2  $\mu\text{A}$ . Activity was extracted and mass separated at the ISOCELE-2 facility, operating on-line to the synchrocyclotron. The mass-separated activity was collected on the aluminized Mylar tape of a fast modular transport sys-

tem. Each source was collected for a preset time and moved to a counting station where its decay was recorded for another preset time. In the reaction, the  $^{133}\text{Pr}$  activity was produced either directly or through the decay of  $^{133}\text{Nd}$  in the target or on the Mylar tape. The collection of the other nuclei along the isobaric chain, Ce, La, and Ba, present in the mass-separated beam was partly discriminated against by the selection of appropriate preset times.

Gamma-ray measurements in the singles and three-parameter  $\gamma$ - $\gamma$ - $t$  coincidence modes were performed using large-volume HPGe coaxial detectors and a HPGe planar detector with a thin Be window. In order to reduce background, some of the singles data were recorded as  $\beta^+$ -gated spectra. A plastic scintillator provided the  $\beta^+$ -coincidence gate. The energy range 10–2500 keV was covered in the present study.

Conversion electrons, singles, and  $e^-$ - $\gamma$ - $t$  were recorded by means of a Si(Li) detector located inside a magnetic selector.<sup>5</sup> The detector was shielded from  $\gamma$ -ray activity, and the selector, in order to record electrons in the range 12–700 keV, was operated at two different fields. The simultaneous recording of  $\gamma$  rays was performed by means of a HPGe detector placed 4 cm away from the source. The geometrical factor required for the conversion-coefficient determinations was initially calculated from the previous measurement of the 172.5-keV  $E3$  isomeric transition in the  $^{127}\text{Xe}$  (on-line  $A = 127$  mass-separated source), and later adjusted by a factor of 0.88 to produce a pure  $E2$  transition for the 241.9 K electrons in the decay of  $^{133}\text{Pr}$ .

## III. RESULTS

The identification of the  $\gamma$  rays following the  $\beta^+$ -EC (electron capture) decay of  $^{133}\text{Pr}$  was based on a previous analysis<sup>6</sup> of mass  $A = 133$  time-multiscale  $\gamma$ -ray spectra, published results,<sup>3</sup> and the coincidence relation with Ce x rays and other  $\gamma$  rays. Shown in Fig. 1 is the low-energy part of the  $\gamma$ -ray spectrum recorded by means of the HPGe planar detector. The energies and relative intensities of the  $\gamma$  rays are listed in Table I together with their placement in the level scheme.

Shown in Fig. 2 is a singles electron spectrum recorded during the  $e^-$ - $\gamma$ - $t$  coincidence measurement. Table II summarizes the results of the conversion-electron mea-

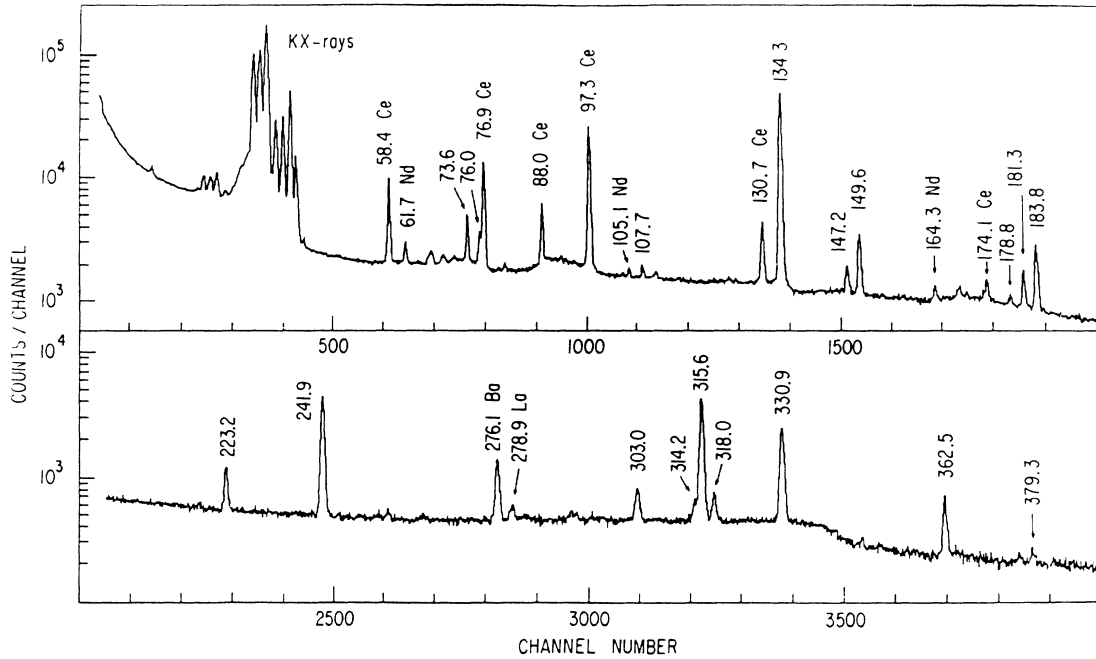


FIG. 1. Low-energy part of  $\gamma$ -ray spectrum associated with the decay of  $^{133}\text{Pr}$ . The energies of the marked peaks are in keV.

TABLE I. Energies and relative intensities of the  $\gamma$  rays observed in the decay of  $^{133}\text{Pr}$  and their placements in the  $^{133}\text{Ce}$  level scheme.

| $E$ (keV) <sup>a</sup> | $I^b$ | $E$ level (keV) | $E$ (keV) <sup>a</sup> | $I^b$ | $E$ level (keV) |
|------------------------|-------|-----------------|------------------------|-------|-----------------|
| 73.6                   | 1.8   | 315.6           | 436.5                  | 2.3   | 570.8           |
| 76.0                   | 1.1   | 318.1           | 461.2                  | 2.5   | 779.3           |
| 107.7                  | 0.4   | 241.9           | 463.4                  | 1.0   | 779.3           |
| 124.4                  | 0.2   | 621.2           | 465.2                  | 61.7  | 465.2           |
| 134.3                  | 100   | 134.3           | 487.1                  | 2.1   | 621.2           |
| 147.2                  | 2.0   | 465.2           | 495.0                  | 1.0   | 1116.2          |
| 149.6                  | 6.4   | 465.2           | 496.4                  | 7.4   | 496.8           |
| 158.4                  | 0.6   | 779.3           | 522.6                  | 1.8   | 656.7           |
| 178.8                  | 0.7   | 496.8           | 537.3                  | 6.1   | 779.3           |
| 181.3                  | 3.7   | 315.6           | 621.4                  | 1.3   | 621.2           |
| 183.8                  | 9.6   | 318.1           | 645.2 <sup>d</sup>     | 11.8  | 779.3           |
| 223.2                  | 5.4   | 465.2           | 653.7                  | 0.7   | 787.5           |
| 241.9                  | 41.9  | 241.9           | 656.7                  | 1.3   | 656.7           |
| 254.8                  | 0.8   | 496.8           | 687.8                  | < 1.6 | 1005.5          |
| 281.5                  | < 0.5 | 902.8           | 689.7                  | 4.2   | 1005.5          |
| 290.6                  | < 0.5 | 787.5           | 700.5                  | 2.3   | 834.9           |
| 303.0                  | 8.0   | 621.2           | 714.0                  | 1.1   | 1335.2          |
| 314.2                  | 4.5   | 779.3           | 779.4                  | 2.6   | 779.3           |
| 315.6                  | 88.1  | 315.6           | 834.9                  | 2.4   | 834.9           |
| 318.0                  | 7.4   | 318.1           | 1005.5                 | 1.4   | 1005.5          |
| 330.9                  | 51.5  | 465.2           | 1076.6                 | 0.3   | 1573.4          |
| 340.9                  | 0.8   | 656.7           | 1386.8                 | 0.7   | 1521.1          |
| 362.5                  | 13.6  | 496.8           | 1639.3                 | 0.5   | 1881.3          |
| 379.3                  | 2.3   | 621.2           | 1747.1                 | 0.4   | 1881.3          |
| 414.5 <sup>c</sup>     | 1.0   | 656.7           |                        |       |                 |

<sup>a</sup>The energies are accurate to  $\pm 0.2$  keV.

<sup>b</sup>Gamma-ray intensities normalized to 100 for the 134.3-keV  $\gamma$  ray. Errors for most intensities are less than 10%.

<sup>c</sup>Corrected for 414  $\gamma$  ray in  $^{133}\text{Nd}$  decay.

<sup>d</sup>Corrected for (465.2 + 134.3) sum peak.

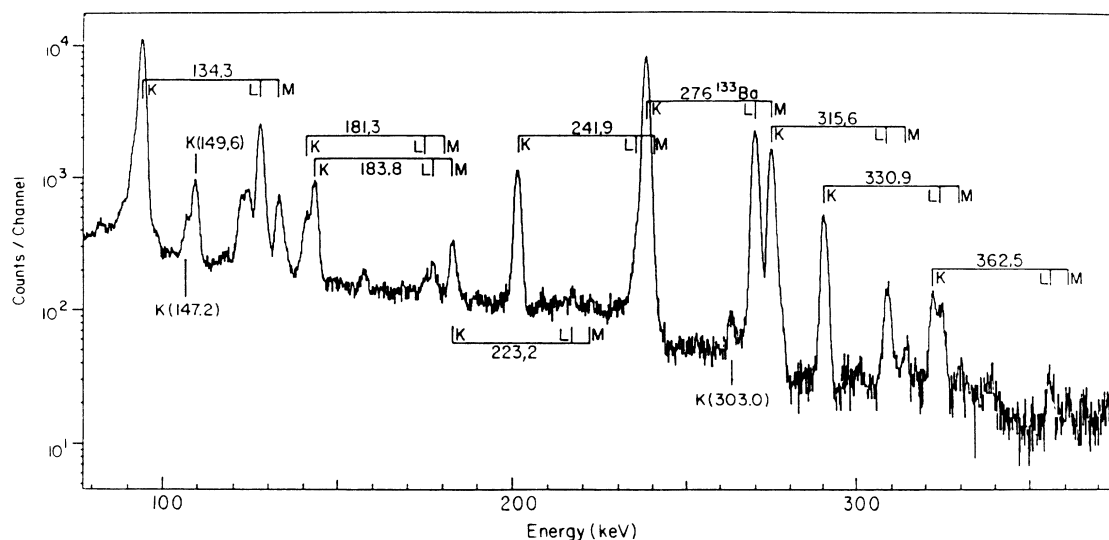


FIG. 2. Conversion electron spectrum in the range 80–380 keV (high-magnetic-field setting) of  $^{133}\text{Pr}$  decay.

measurements and the deduced  $\gamma$ -ray transitions multiplicities. For some of the transitions, due to the complexity of the electron spectrum, the conversion-electron intensities have been obtained from the  $e^- - \gamma - t$  data.

The unavoidable presence of  $^{133}\text{Ce}$  in the mass-separated  $^{133}\text{Pr}$  sources prevented the determination, us-

ing the filtration method,<sup>8</sup> of the branch corresponding to ground-state (g.s.) decay. Therefore,  $\log ft$  values were not calculated.

The decay scheme of  $^{133}\text{Pr}$  obtained from the present work is shown in Fig. 3. Most of the decay feeds the positive-parity levels, which in turn depopulate by transi-

TABLE II. Experimental and theoretical internal conversion-coefficient values and deduced multiplicities.

| Electron line <sup>a</sup> | $\alpha_{\text{expt}}^b$ | $\alpha_{\text{theory}}^c$ |         |         |         | Mult.  |
|----------------------------|--------------------------|----------------------------|---------|---------|---------|--------|
|                            |                          | E1                         | E2      | M1      | M2      |        |
| 73.6 L                     | 0.29(12)                 | 0.067                      | 2.74    | 0.344   | 7.49    | M1     |
| 134.3 K                    | 0.45(7)                  | 0.093                      | 0.492   | 0.449   | 3.23    |        |
| L                          | 0.046(12)                | 0.013                      | 0.184   | 0.061   | 0.656   |        |
| M                          | 0.013(4)                 | 0.0036                     | 0.053   | 0.016   | 0.174   |        |
| K/L/M <sup>d</sup>         | 1/0.11                   | 1/0.137                    | 1/0.374 | 1/0.137 | 1/0.203 | M1     |
|                            | /0.026                   | /0.039                     | /0.108  | /0.035  | /0.054  |        |
| 181.3 L                    | 0.026(12)                | 0.0044                     | 0.053   | 0.027   | 0.174   | M1     |
| 183.8 L                    | 0.028(9)                 | 0.0043                     | 0.050   | 0.026   | 0.166   | M1     |
| 223.2 K <sup>e</sup>       | 0.092(23)                | 0.023                      | 0.098   | 0.111   | 0.555   |        |
| L                          | 0.023(7)                 | 0.0031                     | 0.023   | 0.015   | 0.097   | E2     |
| 241.9 K                    | 0.077(11)                | 0.019                      | 0.077   | 0.089   | 0.427   |        |
| K/L + M <sup>d,f</sup>     | 3.20(96)                 | 6.10                       | 3.57    | 5.73    | 4.74    | E2     |
| 303.0 K                    | 0.015(5)                 | 0.010                      | 0.038   | 0.049   | 0.204   | E1     |
| 315.6 L                    | 0.0060(15)               | 0.0012                     | 0.0064  | 0.0059  | 0.025   |        |
| K/L <sup>d,g</sup>         | 9.51(1.90)               | 7.60                       | 5.21    | 7.47    | 7.12    | M1     |
| 330.9 K                    | 0.041(6)                 | 0.0084                     | 0.029   | 0.039   | 0.154   |        |
| L                          | 0.0071(21)               | 0.0011                     | 0.0054  | 0.0052  | 0.024   |        |
| K/L <sup>d</sup>           | 7.73(1.93)               | 7.65                       | 5.36    | 7.48    | 6.31    | M1     |
| 362.5 K <sup>h</sup>       | 0.045(13)                | 0.0067                     | 0.022   | 0.031   | 0.166   |        |
| L                          | 0.0051(18)               | 0.0009                     | 0.0040  | 0.0041  | 0.018   | M1     |
| 465.2 L                    | 0.016(3)                 | 0.0037                     | 0.011   | 0.016   | 0.054   | M1(E2) |
| 537.3 K                    | 0.013(5)                 | 0.0027                     | 0.0076  | 0.011   | 0.035   | M1(E2) |
| 645.2 K                    | 0.0043(22)               | 0.0018                     | 0.0047  | 0.0073  | 0.021   | (E2)   |

<sup>a</sup>The conversion-electron lines are denoted by  $\gamma$ -ray energy and electron shell.

<sup>b</sup> $\alpha_{\text{expt}}$  values normalized to the theoretical E2 value of 241.9 K.

<sup>c</sup>Theoretical internal conversion coefficients (Ref. 7).

<sup>d</sup>Ratio obtained from  $e^- - \gamma - t$  data.

<sup>e</sup> $\alpha_k$  corrected for 183.8 M electrons.

<sup>f</sup>In the singles spectrum, 241.9 L electrons are not resolved from the intense 276.1 K ( $^{133}\text{Ba}$  decay) electrons.

<sup>g</sup>In the singles spectrum, 315.6 K electrons are not resolved from the intense 276.1 M ( $^{133}\text{Ba}$  decay) electrons.

<sup>h</sup> $\alpha_k$  corrected for 330.9 L electrons.

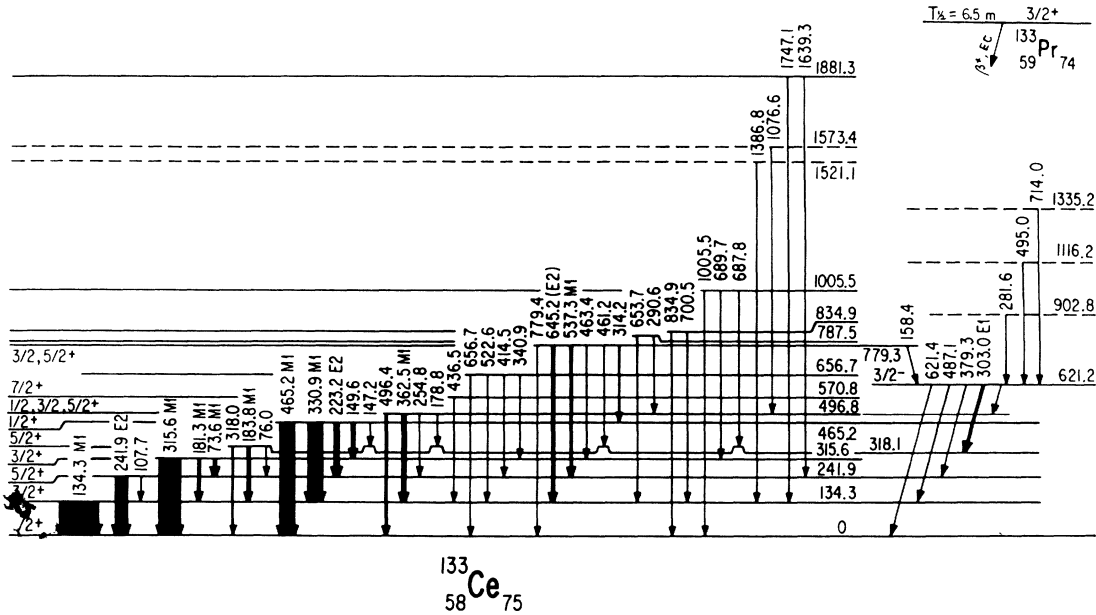


FIG. 3. Decay scheme of  $^{133}\text{Pr}$ . The relative total transition intensities are indicated by the black arrows.

tions down to the g.s. Some of these levels were previously known;<sup>2,3</sup> together with the additional levels deduced in the present study, a correct and detailed decay scheme was constructed.  $^{133}\text{Pr}$  having a spin value of  $\frac{3}{2}^+$  feeds only low-spin levels in  $^{133}\text{Ce}$ . Three of these levels, at 134.3, 318.1, and 570.8 keV, were observed in in-beam study<sup>2</sup> and were assigned  $I^\pi$  values of  $\frac{3}{2}^+$ ,  $\frac{5}{2}^+$ , and  $\frac{7}{2}^+$ , respectively. The first two  $I^\pi$  values are confirmed by the deduced transition multiplicities; no conversion-electron data are available for the third level.

The three excited states at 241.9, 315.6, and 465.2 keV, not observed in the in-beam work, are strongly fed in the decay of  $^{133}\text{Pr}$ . The spin and parity for the level at 241.9 keV were established from the deduced  $E2$  multipolarity of the 241.9-keV transition to the  $\frac{1}{2}^+$  g.s. to be  $\frac{5}{2}^+$ . The level at 315.6 keV depopulates by three  $M1$  transitions to  $\frac{1}{2}^+$ ,  $\frac{3}{2}^+$ , and  $\frac{5}{2}^+$  levels and thus is assigned a  $\frac{3}{2}^+$  value. The level at 465.2 keV depopulates by two  $M1$  transitions to  $\frac{1}{2}^+$  and  $\frac{3}{2}^+$  levels and by  $E2$  transition to a  $\frac{3}{2}^+$  level and thus is assigned a  $\frac{1}{2}^+$  value. The lack of complete electron data for the rest of the transitions does not allow exact additional  $I^\pi$  values assignment. However, suggestions concerning  $I^\pi$  values for some of the levels are included in the level scheme.

A very small fraction of the  $^{133}\text{Pr}$  decay feeds a level at 621.2 keV and three additional levels at higher energies. Negative parity was deduced for the level at 621.2 keV, which populates the  $\frac{5}{2}^+$  level by a 303.0  $E1$  transition. For the same level, transitions of undetermined multiplicities to the  $\frac{1}{2}^+$ ,  $\frac{3}{2}^+$ , and  $\frac{5}{2}^+$  levels suggest a spin value of  $\frac{3}{2}^-$ . The other three levels that solely populate the  $\frac{3}{2}^-$  level have probably negative parities. Contrary to the level structure of positive parity, the negative levels do not populate the respective low-lying  $I^\pi = \frac{9}{2}^-$  isomeric state, which indicates spin values smaller than  $\frac{5}{2}$ .

#### IV. DISCUSSION

The following discussion is mainly concerned with the low-energy levels of  $^{133}\text{Ce}$  observed and characterized in some detail in the present experimental study. A few high-spin states observed in heavy-ion gamma-ray spectroscopy<sup>2</sup> and constituted into bands built on low-lying states are also considered. There are two such bands, one of positive parity based on the  $\frac{1}{2}^+$  ground state (Fig. 4), and one of negative parity based on the  $E_x = 39$  keV,  $\frac{9}{2}^-$  state<sup>2</sup> (Fig. 5).

A description of these states is proposed in the frame of the interacting boson-fermion model, in its version which does not distinguish the neutrons and protons (IBFM-1).<sup>9</sup> The  $^{133}\text{Ce}$  nucleus is considered as a  $^{134}\text{Ce}$  core, described by the IBA-1 model, to which one couples a neutron hole. The model parameters were determined by starting from those of the isotonic nucleus  $^{131}\text{Ba}$ , which were found in a recent consistent IBFM-1 description of the neutron-deficient Ba isotopes 123–131.<sup>10</sup> The odd fermion is allowed to occupy the following shell model orbitals:  $2d_{5/2}$ ,  $1g_{7/2}$ ,  $3s_{1/2}$ ,  $2d_{3/2}$ ,  $1h_{11/2}$ ,  $2f_{7/2}$ , and  $1h_{9/2}$ . Use was made of Scholten's parametrization<sup>11</sup> for the boson-fermion interaction part of the Hamiltonian, with a realistic scheme of the neutron single-particle energies in  $A \approx 130$  nuclei, such as provided by Nilsson<sup>12</sup> or Woods-Saxon<sup>13</sup> potentials. The single-particle energies are (all in MeV, relative to the  $d_{5/2}$  orbital)  $g_{7/2}$ , 0.6;  $s_{1/2}$ , 2.3;  $d_{3/2}$ , 2.6;  $h_{11/2}$ , 2.7;  $f_{7/2}$ , 5.8; and  $h_{9/2}$ , 5.9. A BCS calculation provided the quasiparticle energies and the shell occupation probabilities needed in the Hamiltonian parametrization,<sup>11</sup> which were then used in the calculation of the levels of both parities. The Hamiltonian contains finally three parameters,  $A_0$ ,  $\Gamma_0$ , and  $\Lambda_0$ , which determine the intensities of the monopole, quadrupole, and exchange forces, respectively, and are determined

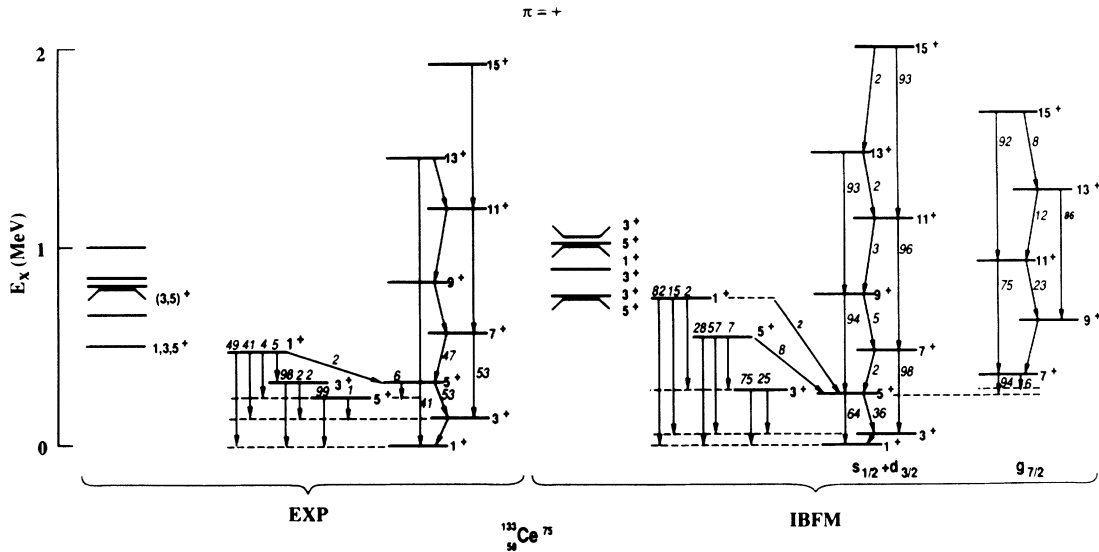


FIG. 4. Experimental and theoretically predicted (IBFM-1) positive-parity levels in  $^{133}\text{Ce}$ . Gamma-ray transitions are labeled by their branching ratios, the experimental ones being determined from the present  $\gamma$ -ray intensities and those of Ref. 2. Only the branches larger than 2% are shown. Shown separately on the left-hand side of each level scheme are the rest of the levels populated in the  $^{133}\text{Pr}$  beta decay and the rest of predicted levels with spin  $\frac{1}{2}$ ,  $\frac{3}{2}$ , and  $\frac{5}{2}$ , respectively, all up to  $E_x \approx 1$  MeV. The two theoretical bands are labeled by the shell-model orbitals which dominate the structure of their wave functions. The spins are specified by the double of their value.

such as to describe the experimental level scheme (separately for the two parities). The calculations were performed with the code ODDA.<sup>14</sup>

The comparison between the calculated and experimental level and decay schemes is shown in Figs. 4 and 5. The theoretical gamma-ray branching ratios are determined from calculated absolute  $B(E2)$  and  $B(M1)$  reduced transition probabilities. The parameters of the  $E2$

and  $M1$  transition operators<sup>15</sup> have been determined as follows. For the  $E2$  transition operator, the boson effective charge  $e_B = 0.13 e b$  was determined from the  $B(E2; 2_1^+ \rightarrow 0_{g.s.}^+)$  values known in the neighboring Ce and Ba isotopes.<sup>16</sup> Since the fermionic part of the transition operator contributes very little in comparison with the bosonic one the fermionic effective charge  $e_F$  was taken equal to  $e_B$ . The  $\chi$  value from the quadrupole boson operator is the same as that from the Hamiltonian ( $\chi = -1.1$ ).

The boson gyromagnetic factor  $g_d = 0.3 \mu_N$ , as resulting from known magnetic moments of the  $2_1^+$  state in the  $^{130-134}\text{Ba}$  isotopes,<sup>17</sup> was used for the  $M1$  transitions. For the fermionic part of the  $M1$  operator  $g_1 = 0$  was chosen (the odd particle is a neutron) and  $g_s = -1.15 \mu_N$ , as determined<sup>10</sup> by fitting different known magnetic moments of low-lying states (of both parities) in the odd Ba isotopes 125–131.<sup>17</sup> In deducing the theoretical gamma-ray branchings, use was made of the experimental gamma-ray energies whenever it was considered that there was an obvious correspondence between the calculated levels and known experimental levels; when the experimental levels were missing the theoretical gamma-ray energies were used.

A comparison of the known positive-parity states with the IBFM-1 calculations is shown in Fig. 4. Both the position of the levels and their gamma-ray decays are reasonably well reproduced. The states in the band based on the  $\frac{1}{2}^+$  ground state have mixed wave functions, whose structure is dominated by the  $s_{1/2}$  and  $d_{3/2}$  orbitals. The additional lowest  $\frac{5}{2}^+$ ,  $\frac{3}{2}^+$ , and  $\frac{1}{2}^+$  states have wave functions of similar character, and are consequently connected by multiple transitions with states in the g.s.

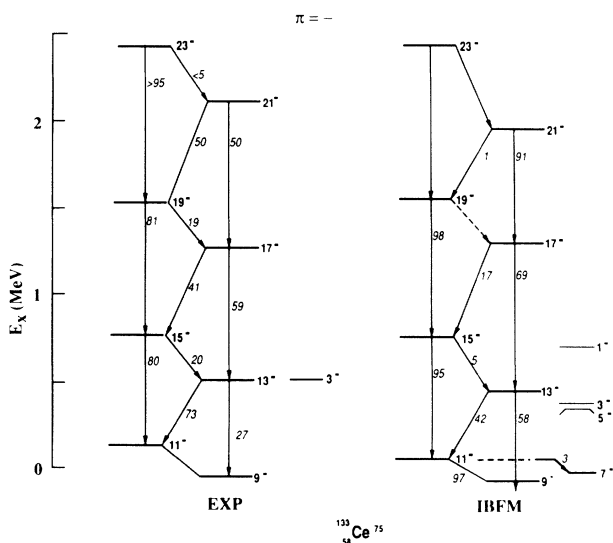


FIG. 5. Similar to Fig. 4 but for the negative-parity levels in  $^{133}\text{Ce}$ . The excitation energies are given relatively to the  $\frac{9}{2}^-$  state. The experimental branching ratios are based on the data of Ref. 2.

band, as observed experimentally. All the remaining levels of, presumably, positive parity observed experimentally up to 1-MeV excitation are also given in the figure. Since one may assume that mainly states of spin  $\frac{1}{2}$ ,  $\frac{3}{2}$ , and  $\frac{5}{2}$  are populated in the  $\beta$  decay of  $^{133}\text{Pr}(\frac{3}{2}^+)$ , all the theoretically predicted levels with these spin values up to  $E_x \approx 1$  MeV are also shown separately in Fig. 4. There is a reasonable correspondence between these levels and the experimentally observed group of levels, both in number and excitation energy. The model parameters for the positive-parity level scheme in Fig. 4 are  $A_0 = -0.15$  MeV,  $\Gamma_0 = 0.49$  MeV,  $\Lambda_0 = 1.0$  MeV; only the value of the exchange force parameter  $\Lambda_0$  differs from that determined for the isotonic nucleus  $^{131}\text{Ba}$  (0.5 MeV).<sup>10</sup>

The calculations also predict a low-lying band based on a  $\frac{7}{2}^+$  state (also shown in Fig. 4), similar to the Ba isotopes where this band has been determined experimentally for  $N < 75$ .<sup>10</sup> The structure of this band is predominantly  $g_{7/2}$ . The position of its head is strongly dependent on the energy of the  $g_{7/2}$  single-particle state, relative to the  $d_{5/2}$  one (the  $s_{1/2}$ - $d_{3/2}$  structures discussed above being rather insensitive to this parameter), and somewhat on the value of  $\Lambda_0$ . Since this band has not yet been observed, there is still a place for a better determination of these model parameters. According to the present calculations, the  $\frac{7}{2}^+$  head of this  $g_{7/2}$  band must lie not too far from the known  $\frac{7}{2}^+$  state and should be an

isomeric state. (Without taking into consideration the internal conversion, a lifetime of about 0.5  $\mu\text{s}$  was estimated.)

The negative-parity level scheme under discussion is shown in Fig. 5, in comparison with the IBFM calculation. The model parameters, determined from a fit to the yrast levels, are  $A_0 = -0.24$  MeV,  $\Gamma_0 = 0.68$  MeV, and  $\Lambda_0 = 1.74$  MeV. They are practically identical to those determined for the  $^{131}\text{Ba}$  nucleus.<sup>10</sup> The structure of the negative parity is dominated by the  $h_{11/2}$  orbital. The calculations predict reasonably well the  $\frac{3}{2}^-$  state experimentally determined at  $E_x = 583$  keV. The lowest predicted  $\frac{1}{2}^-$ ,  $\frac{5}{2}^-$ , and  $\frac{7}{2}^-$  states are also given in Fig. 5.

The relative position of the positive- and negative-parity levels is also correctly reproduced: The  $\frac{9}{2}^-$  level is predicted 58 keV less bound than the  $\frac{1}{2}^+$  state, which compares well with the experimental value  $E_x = 39$  keV.

The general features of the observed decay schemes for both the positive- and negative-parity states (Figs. 4 and 5) are reproduced. The comparison shows, however, that the  $M1$  transitions between the favored and unfavored members of the bands are underestimated. In the absence of gamma-ray transition probabilities it is difficult to decide whether this is due to details of the wave functions, to the need for other values for the  $M1$  transition operator parameters, or to the form of the  $M1$  operator itself.<sup>18</sup>

\*Present address: Soreq Nuclear Research Center, Yavne 70600, Israel.

†Present address: Institute of Atomic Physics, P.O. Box MG-6, Bucharest, Romania.

<sup>1</sup>R. Moscrop, M. Campbell, W. Gellety, L. Goetting, C. J. Lister, and B. J. Varley, Nucl. Phys. **A481**, 559 (1988), and references therein.

<sup>2</sup>R. Ma, E. S. Paul, C. W. Beausang, S. Shi, N. Xu, and D. B. Fossan, Phys. Rev. C **36**, 2322 (1987).

<sup>3</sup>Yu. V. Sergeenkov and V. M. Sigalov, Nucl. Data Sheets **49**, 639 (1986).

<sup>4</sup>S. Ingelman, C. Ekstrom, M. Olsmats, and B. Wannberg, Phys. Scr. **7**, 24 (1973).

<sup>5</sup>P. Paris and J. Treherne, Rev. Phys. Appl. **4**, 291 (1969).

<sup>6</sup>C. F. Liang, P. Paris, D. Bucurescu, and M. S. Rapaport, Phys. Rev. C **40**, 2796 (1989).

<sup>7</sup>F. Rosel, H. M. Fries, and K. Alder, At. Data Nucl. Data Tables **21**, 236 (1978).

<sup>8</sup>B. Pfeiffer, J. P. Bocquet, A. Pinston, R. Roussille, M. Asghar, G. Bailleul, R. Decker, J. Greif, H. Scharder, G. Siegart, H.

Wollnik, J. Blachot, E. Monnard, and F. Schussler, J. Phys. (Paris) **38**, 9 (1977).

<sup>9</sup>F. Iachello and O. Scholten, Phys. Rev. Lett. **43**, 679 (1979).

<sup>10</sup>D. Bucurescu, G. Cata, A. Gizon, J. Gizon, and N. V. Zamfir, in Proceedings of the Oak Ridge Conference on Nuclear Structure in the Nineties, Oak Ridge, 1990 (Report CONF-900450).

<sup>11</sup>O. Scholten, Ph.D. thesis, University of Groningen, 1980.

<sup>12</sup>A. Bohr and B. R. Mottelson, *Nuclear Structure* (Benjamin, New York, 1974), Vol. II.

<sup>13</sup>W. Nazarewicz, J. Dudek, R. Bengtsson, T. Bengtsson, and I. Ragnarsson, Nucl. Phys. **A435**, 397 (1985).

<sup>14</sup>O. Scholten, Kernphysisch Versneller Institut, Internal Report KVI252, 1982 (unpublished).

<sup>15</sup>O. Scholten and T. Ozzello, Nucl. Phys. **A424**, 221 (1984).

<sup>16</sup>S. Raman, C. W. Nestor, S. Kahane, and K. H. Bhatt, At. Data Nucl. Data Tables **42**, 1 (1989).

<sup>17</sup>P. Raghavan, At. Data Nucl. Data Tables **42**, 189 (1989).

<sup>18</sup>L. D. Wood and I. Morrison, J. Phys. G **15**, 997 (1989).